ACS APPLIED MATERIALS & INTERFACES

Research Article

www.acsami.org

Stable, High-Efficiency Pyrrolidinium-Based Electrolyte for Solid-State Dye-Sensitized Solar Cells

Tong He,[‡] Ye Feng Wang,[*,†,§] and Jing Hui Zeng[*,‡,§]

[†]School of Chemistry & Chemical Engineering, [‡]School of Material Science and Engineering, and [§]Shaanxi Provincial Key Laboratory of Macromolecular Science, Shaanxi Normal University, Xi'an 710620, P. R. China

Supporting Information

ABSTRACT: We synthesized a series of pyrrolidinium based dicationic ionic crystals with high melting point and good thermal stability. Research on the crystal structure shows that there are ordered three-dimensional ionic channels in these crystals which is favorable for the ionic conductor to achieve high conductivity and diffusion coefficient. These ionic crystals are applied to electrolyte as matrix in dye sensitized solar cells, and the influence of crystal structure (including the alkylene chain separating two pyrrolidinium rings and anion) versus the device performances are studied by steady-state voltammography, current−voltage trace, and electrochemical impedance spectroscopy. As the solid state electrolyte, an optimized efficiency of 6.02% have achieved under full sunlight irradiation using ionic crystal $[C_6BEP]$-$[TFSI]_2$. And the device based on this solid electrolyte shows the excellent long-term stability, maintaining 92% of the initial efficiency after 960 h. This study elucidates fundamental the structure of dicationic crystal and provide useful clues for further improvement of solid-state electrolytes in DSSC.

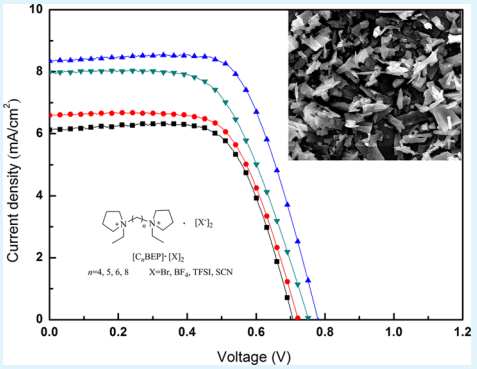

KEYWORDS: *three-dimensional channel, organic ionic-conductor, dicationic, electrolyte, DSSC*

INTRODUCTION

Solid-state dye-sensitized solar cells (ssDSSCs) have attracted much research attention these days because they can overcome the potential problems of leaking and sealing, flammability issues, and electrochemical instability accompanied by the liquid electrolytes.[1−3] Thus, quasi-solid polymer electrolytes and solid inorganic semiconductors were used as the alternatives to liquid electrolyte.[4−8] However, because of the thermodynamical instability of quasi-solid electrolytes under the repeated exposure to solar heating[3,9,10] (>70 °C for up to 10% of their operating life[11]) and the poor interfacial contact of inorganic conductors arising from the fast crystal growth of the inorganic materials, it is still a great challenge to develop efficient and stable solid electrolyte materials.

Organic ionic crystals (OICs) are a kind of crystalline compounds containing anions and cations whose properties differ from those of the conventional crystals.[12] In term of structure, they are the solid-state analogues of ILs. On the other hand, they overcome the fluidity of ionic liquids with holding their unique suite of properties such as low volatility, low flammability, and high chemical and electrochemical stability.[13] Although the ionic crystals themselves usually suffer from low conductivity, they can provide the mechanism for fast conduction of the doped ions as a chemically inert matrix.[14] In view of the above ionic character, organic ionic crystals are ionic conductors and a promising candidate for solid electrolytes in DSSCs. Particularly compared with quasi-solid electrolytes and inorganic semiconductors, these crystals show theoretically the better thermal-stability and excellent adjustability of structure according to the request. However, the research on OICs is still in the early stage, and sorts of compounds involved in this field is extremely limited. So far, most of the types of OICs are confined to the imidazolium-based compounds, such as 1-methyl-3-acetylimidazolium iodide (MA-II),[15] *N*-propargyl imidazolium,[14] carbazole-imidazolium iodide,[16] cyanobiphenyl-functionalized imidazolium,[12] and ester-functionalized imidazolium.[17−20] Therefore, the primary issue is enriching the species of OICs to make in-depth research on the solid electrolytes based on OICs.

In contrast with imidazolium, pyrrolidinium possess the better electrochemical stability because of its nonaromatic character.[21] And the excellent electrochemical properties have made them have wide application in the lithium battery[22,24] and quantum dot-sensitized solar cell.[25] However, only few pyrrolidinium-based OICs have been synthesized and applied in ssDSSCs such as *N*,*N* -dimethylpyrrolidinium dicyanamide ($[C_1mpyr][N(CN)_2]$),[26] 1-methyl-1-ethylpyrrolidinium bis-(trifluoromethanesulfonyl)imide ($P_{12}TFSI$),[27] and 1-methyl-1-ethylpyrrolidinium iodide ($P_{12}I$).[28]

In this work, we synthesized a novel kind of pyrrolidinium-based OICs on the basis of our early research work about the dictionic OICs (Figure 1).[29] Through analyzing the crystal

Received: July 8, 2015
Accepted: September 3, 2015
Published: September 3, 2015

© 2015 American Chemical Society

DOI: 10.1021/acsami.5b06035
ACS Appl. Mater. Interfaces 2015, 7, 21381−21390

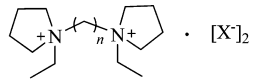

$[C_nBEP]\cdot[X]_2$

n=4, 5, 6, 8 X=Br, BF_4, TFSI, SCN

Figure 1. Chemical structures of the pyrrolidinium-based dicationic crystals.

structure, there are ordered three-dimensional ionic channels in these crystals, which is favorable for the ionic conductor to achieve high conductivity and diffusion coefficient. We applied these crystals as electrolyte matrix into ssDSSCs and achieved photoelectric conversion efficiency of 6.02% under full air-mass (AM 1.5) sunlight (100 $mW\cdot cm^{-2}$), superior to those of devices with other pyrrolidinium-based OICs reported.

EXPERIMENTAL SECTION

Materials and Reagents. Pyrrolidine, bromoethane, 1,4-dibromobutane, 1,5-dibromopentane, 1,6-dibromohexane, 1,8-dibromooctane, 1-ethyl-3-methylimidazolium iodide (EMII), 1-methyl-3-propylimidazolium iodide (MPII), 1,2-dimethyl-3-propylimidazolium iodide (DMPII), 4-*tert*-butylpyridine (TBP), lithium iodide, potassium hexafluorophosphate, and LiTFSI were purchased from Aladdin Industrial Co. and used without any processing. Iodine, potassium tetrafluoroborate, and H_2PtCl_6 (AR) were purchased from Sinopharm Chemical Reagent Co., Ltd.. Organic solvents used in this work were purified using the standard process. FTO transparent conductive glass was used as the substrate for fabrication of TiO_2 thin film electrode and purchased from Wuhan Geao Science Instruments Co.. $TiCl_4$ (AR) and dye sensitizer (N719) were purchased from Tianjin Kemiou Chemical Reagent Co., Ltd. and Wuhan Jingge Solar Energy Tech. Co., Ltd., respectively. P25 particles were obtained from Evonik Degussa (China) Co., Ltd..

Synthesis of Ionic Crystals. The *N*-ethylpyrrolidine was prepared according to the literature.[30] The synthesis of ionic crystals was achieved in two steps: the coupling reaction of *N*-ethylpyrrolidine with a dibromoalkane and the anion exchange in suitable solvent. Bis(*N*-ethylpyrrolidinium)dibromides were synthesized as follows: 11 mL (0.09 mol) of *N*-ethylpyrrolidine and 0.03 mol of dibromoalkane were added into 50 mL of acetone. The resulting solution was stirred at 90 °C for 72 h. The resulting mixture was filtered to obtain the white precipitant. The crude product was washed successively by acetone, petroleum ether and diethyl ether. The pure products were obtained after vacuum drying at 40 °C for 24 h. ^{1}H NMR of all the dicationic crystals involved in the article (as shown in Figures S1–S10); ^{13}C NMR of $[C_nBEP][Br]_2$ (n = 4, 5, 6, 8) (as show in Figure S1–S4 in Supporting Information); ESI - MS of $[C_nBEP][Br]_2$ (n = 4, 5, 6, 8) (as show in Figure S1 - S4 in Supporting Information). The anion exchange step was achieved by a metathesis reaction of the bromide salts with the corresponding anion salts. 0.003 mol of bromide salts were dissolved in 10 mL of solvent (H_2O or acetone) and treated with 0.015 mol of corresponding anion salt. The resulting solution was stirred at room temperature for 24 h. The solvent was removed by evaporation under reduced pressure. And the final product (white solid) was dried under vacuum at 40 °C for 24 h. ^{1}H NMR of $[C_nBEP][BF_4]_2$ (n = 4, 5, 6, 8) (as shown in Figures S5–S8); ^{1}H NMR of $[C_6BEP][X]_2$ (X = SCN^-, $TFSI^-$) (as shown in Figures S9 and S10); IR spectra for $[C_nBEP][Br]_2$, $[C_nBEP][BF_4]_2$ (n = 4, 5, 6, 8) and $[C_6BEP][X]_2$ (X = SCN^-, $TFSI^-$) (as shown in Figure S11).

Preparation of Electrolytes. The electrolyte was made up with four parts: ionic crystal matrix, I^- source (DMPII or EMII), I_2 and charge recombination inhibitor (TBP). All components were mixed in the relevant molar proportion 0.1:0.1:0.02:0.01 and uniformly ground. Then a solid-state electrolyte was obtained before the characterization and fabrication of DSSC.

Device Fabrication of DSSC. FTO conductive glass was successively washed by hydrochloric acid, ethanol, isopropanol and distilled water in ultrasonic clearing machine for 30 min. The $TiCl_4$ aqueous solution with 0.05 mol/L of concentration was prepared at 0 °C. The glass substrate was treated with the above $TiCl_4$ aqueous solution at 80 °C for 1 h to make TiO_2 particles deposited onto the FTO conductive glass, and then the compact TiO_2 layer was produced. The FTO conductive glass was covered at two parallel edges with an adhesive tape to shape a 1 cm × 1 cm area. The thick film of 20 nm sized P25 particles was deposited onto the FTO conductive glass electrode by the doctor-blade technique. The resulting TiO_2 film was annealed at 450 °C for 30 min, by which the mesoporous TiO_2 film was formed. The obtained TiO_2 electrode was cooled to 80 °C and immersed in N719 ethanol solution with 0.5 mol/L of concentration at room temperature for 15 h to complete the sensitizer loading. The dye-sensitized TiO_2 electrode was washed with anhydrous ethanol to remove the nonabsorbed dye and dried in vacuum drying oven.

The Pt counter electrode was prepared with pyrolysis method. The 0.05 mol/L H_2PtCl_6 isopropanol solution was put onto the cleaned FTO conductive glass substrate. After it dried completely in the air, the resulted FTO conductive glass was annealed at 380 °C for 30 min. The above procedure was repeated twice, and then the Pt counter electrode was eventually formed.

Solid-state dye-sensitized solar cell was fabricated by sandwiching the ionic crystals-based electrolytes into the space between the dye-sensitized TiO_2 electrode and the Pt counter electrode using the knife coating method to form a 1 cm^2 area sheet. The two electrodes were clipped together by hot press (under 0.18 MPa of pressure at 135 °C for 35 s) and a 100 μm thick heat-sealing film was used for the sealing of the cell.

Characterization. ^{1}H NMR and ^{13}C NMR were characterized with a Bruker Avance 400 MHz spectrometer. And IR spectra were recorded on a Bruker Tensor 27 spectrometer. The molecular weights were confirmed by MALDI-TOF Bruker mass spectrometer. The XRD

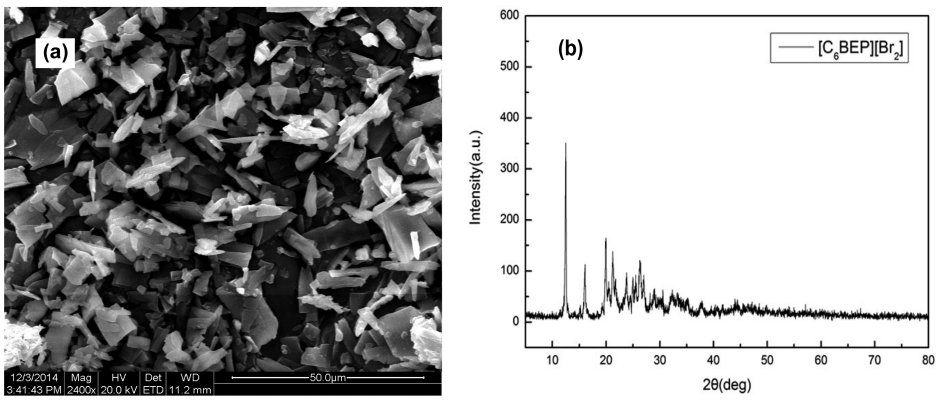

Figure 2. (a) SEM image and (b) XRD pattern of crystals $[C_6BEP][Br]_2$.

DOI: 10.1021/acsami.5b06035
ACS Appl. Mater. Interfaces 2015, 7, 21381–21390

measurements were performed on a Rigaku D/Max-RA X-ray diffractometer equipped with graphite-monochromatized high-intensity Cu Kα radiation (λ = 1.5418 Å). Single crystal was obtained from ethanol at room temperature and measured on an Oxford GEMINI E X-ray single crystal diffractometer. The surface morphology was determined by a scanning electron microscope (SEM). The thermal properties of crystals were measured with a Thermoanalyzer Systems (Q1000DSC+LNCS+FACS Q600SDT) at a scanning rate of 10 °C/min in the temperature range of 20−600 °C under N_2 atmosphere.

The ionic conductivity of the ionic crystals electrolytes was determined by the electrochemical impedance measurements with an ordinary cell composed of Teflon tube and two conductive glass electrodes which were a square with 1 cm^2 on the side on a CHI660d electrochemical workstation at room temperature over the frequency range of 1 MHz to 1 Hz. The steady-state voltammetry was tested in an electrochemical cell equipped with a 0.05 mm radius platinum ultramicroelectrode as the working electrode, a platinum foil as the counter electrode, and a saturated calomel electrode as reference electrode.

The photocurrent intensity vs. photovoltage (J−V) curves of the devices were acquired with a Keithley 2400 source meter under standard AM 1.5 solar illuminations at intensity of 100 mW cm^{-2}. The electrochemical impedance spectra (EIS) for devices were tested with an CHI660d electrochemical workstation equipped with three identical stainless steel electrodes as the working, counter and reference electrodes, respectively, under dark state. The spectra were performed at various forward bias voltages from −0.70 to 0.8 V in the frequency range 1 × 10^5 to 0.01 Hz. Incident monochromatic photocurrent conversion efficiency (IPCE) curves of DSSCs were measured by QTest Station 2000 IPCE Measurement System (Crowntech, USA).

RESULTS AND DISCUSSION

Crystal Structure of Ionic Crystal. The crystal properties of the organic dicationic compounds were confirmed by the SEM images and XRD patterns, as shown in Figure 2 and Figure S12. Figure 2a shows room temperature SEM picture of the pure $[C_6BEP][Br]_2$ as a white solid. From the image, we can see the crystals of $[C_6BEP][Br]_2$ show the slice shape with the crystal sizes from 5.1 to 14 μm. And the textured structure and flat surfaces of $[C_6BEP][Br]_2$ are clear, which can demonstrate the crystal nature of this material. Figure 2b shows the XRD pattern of $[C_6BEP][Br]_2$. The sample shows strong diffraction peaks, which is also a clue for the crystal nature of this material. However, because of the lack of standard diffraction data, the crystal structure can't be determined according to the present patterns.

To clarify the structure of dicationic crystal, we obtained the single crystal of $[C_6BEP][Br]_2$ by slow evaporation of a ethanol solution, as shown in Figure 3. A summary of the crystal data is given in Table 1. To the best of our knowledge, this is the first structural information on this dication. The result of the X-ray analysis of crystal $[C_6BEP][Br]_2$ exhibits the existence of the $[C_6BEP]^{2+}$ dication, two bromide anions, and four water molecules in the unit of a triclinic cell. When the nonaromatic rings are joined to the ends of hexamethylene, the resulting heterocycle shows an elongated shape with two nitrogen atoms, in which the distances for C^1−C^2, C^2−C^3, and C^3−C^4 are 1.5165, 1.5042, and 1.5245 Å, respectively. Considering only 0.2° of the torsion angle for C^1, C^2, C^3, and C^4 (or for $C^{1\alpha}$, $C^{2\alpha}$, $C^{3\alpha}$, and $C^{4\alpha}$), we consider these four carbon atoms to be roughly on the same plane in each pyrrolidinium ring. N^6 and $N^{6\alpha}$ atom lies outside the above plane with the distance of 0.5767 Å in the opposite side. So two pyrrolidinium rings exist in envelope conformation. It is worth noting that the plane including C^1, C^2, C^3, and C^4 is exactly parallel with that of $C^{1\alpha}$, $C^{2\alpha}$, $C^{3\alpha}$, and $C^{4\alpha}$ with the distance of 0.24 Å in each $[C_6BEP]^{2+}$ dication.

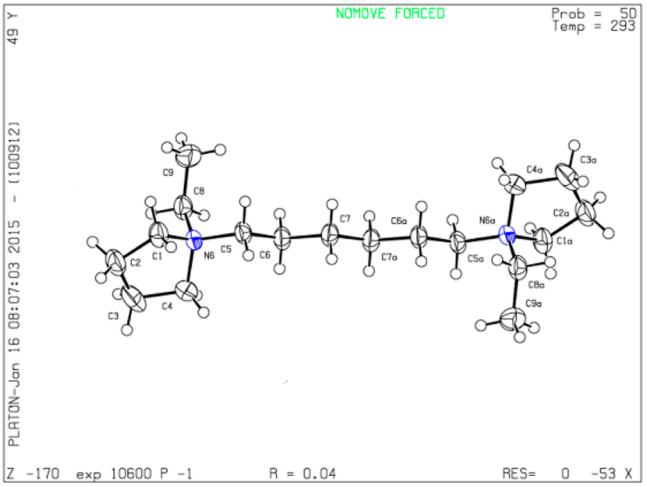

Figure 3. Single-crystal structure of cation of $[C_6BEP][Br]_2$. Hydrogens and bromines are omitted for clarity.

Table 1. Summary of Crystal Data for $[C_6BEP][Br]_2$

cryst syst	triclinic	Z	1
space group	$P\bar{1}$	ρ (calcd) (g/cm^3)	1.373
a (Å)	7.0543 (3)	F (000)	270.0
b (Å)	8.2313 (3)	2θ range (deg)	7.974−144.544
c (Å)	11.3765 (4)	reflns collected	11523
α (deg)	95.832 (3)	GOF on F^2	1.103
β (deg)	99.582 (3)	R_1[a], wR_2[b] [$I \geq 2\sigma(I)$]	0.0370, 0.0972
γ (deg)	104.964 (4)	largest diff peak/hole (e Å^{-3})	0.27/-0.81

[a] $R_1 = \sum ||F_0| - |F_c|| / \sum |F_0|$

[b] $\{R_2 = \sum [w(F_0^2 - F_c^2)^2] / \sum [w(F_0^2)^2]\}^{1/2}$

The crystal structure of $[C_6BEP]^{2+}$ contains only one type of stacking, face-to-face stacking (Figure 4), which is different from that of $[C_3(mpy)_2]^{2+}$ dication (1,1′-(propane-1,3-diyl)-bis(1-methylpyrrolidinium)) with the similar structure synthesized by Armstrong's group.[31] The two pyrrolidinium rings of neighboring molecules are exactly parallel (the dihedral angle between pyrrolidinium rings of different molecules is 0°) and alternately arrange as Figure 4a shown. Ring plane/ring plane distance between pyrrolidinium rings of different molecules are 3.67 and 2.78 Å, respectively. Figure 4b is the packing diagram taken along a-axis of $[C_6BEP]^{2+}$ dication. The perspective view confirms the presence of ordered three-dimensional ionic channels, which is favorable for the ionic conductor to achieve high conductivity.

Thermal Properties of Ionic Crystals. The fundamental thermal properties of dicationic ionic crystals were performed with thermalgravimetric analysis (TGA, 5% weight loss) and differential scanning calorimeter (DSC) (as shown in Figures S13 and S14), and the results were summarized in Table 2.

As depicted in Figures S13a and S14a, TGA curves of $[C_nBEP][Br]_2$ (n = 4, 5, 6, 8) show one stage decomposition behavior. $[C_6BEP][Br]_2$ has the decomposition temperatures at

DOI: 10.1021/acsami.5b06035
ACS Appl. Mater. Interfaces 2015, 7, 21381−21390

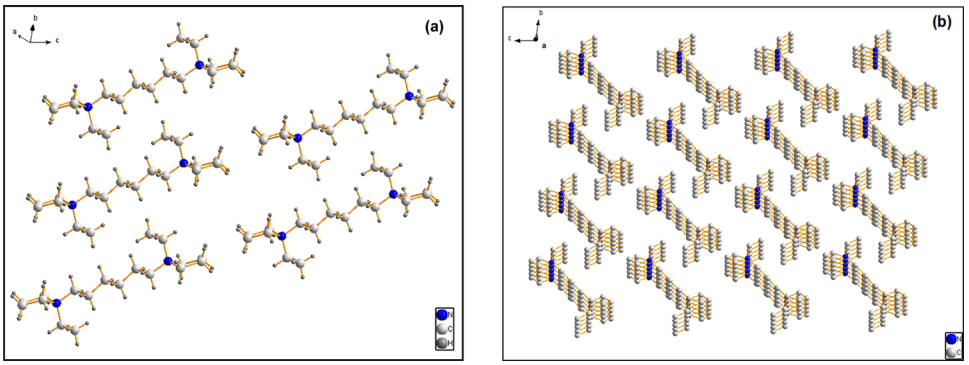

Figure 4. (a) Face-to-face stacking and (b) packing diagram along the *a*-axis for cation of $[C_6BEP][Br]_2$.

Table 2. Thermal and Physical Properties of $[C_nBEP][X]_2$

compd	M_w (g/mol)	appearance (25 °C)	T_m[b] (°C)	T_d[c] (°C)
$[C_4BEP][Br]_2$	414.09[a]	white crystal	163.59	251.15
$[C_5BEP][Br]_2$	428.10[a]	white crystal	243.57	271.64
$[C_6BEP][Br]_2$	442.11[a]	white crystal	[d]	283.05
$[C_8BEP][Br]_2$	470.14[a]	white crystal	[d]	276.71
$[C_6BEP][BF_4]_2$	455.91[a]	white crystal	170.40	289.67
$[C_6BEP][TFSI]_2$	842.60[a]	white crystal	86.46	265.56
$[C_6BEP][SCN]_2$	398.47[a]	white crystal	90.43	411.88

[a]Molecular weight measured by mass spectrometry. [b]Melting point. [c]Decomposition temperature. [d]These compounds decomposed before melting.

approximately 280 °C, and $[C_6BEP][TFSI]_2$ is thermally stable until about 260 °C. So these ionic crystals show good thermal stabilities. The phase transition behaviors for these compounds were examined. As shown in Figures S13b and S14b, these ionic crystals do not exhibit transition behavior in experimental temperature. Most of compounds have melting points above 150 °C, even the lowest melting point that $[C_6BEP][TFSI]_2$ shows is higher than 70 °C (the higher working temperature of DSSC outdoor). From the previous study, structural factors were found to affect the melting point of geminal dicationic compounds: (1) the nature of the dication, (2) the length of the linkage chain separating the geminal dication, and (3) the nature of anion.[31,32] Comparing the melting points of $[C_nBEP][Br]_2$ (n = 4, 5, 6, 8), it is obvious that the spacer length between two pyrrolidinium cations does not play an important role. To see the effect of the anions, we synthesized the bis(pyrrolidinium)hexane salts paired with different anions. In this series of compounds, the melting point of tetrafluoroborate salt is usually higher than those of the Br^-, $TFSI^-$, and SCN^- salts.

Ionic Conductivities and Diffusion Coefficients of Ionic Crystals. Apart from thermal stability, the ionic conductivity is another critical factor for the photovoltaic performances of DSSC.[17] According to our previous work experience, the conductivity of tetrafluoroborate salt is usually superior to those of other salts. Therefore, the ionic conductivities of the pyrrolidinium tetrafluoroborate based ionic crystals with different alkylene linkage chains and different counteranions containing the solar cell additives (not including TBP) were obtained by EIS technique (as presented in Figure 5), and the values were calculated according to the equation inserted in Figure 5a, where σ is the conductivity in S/cm, R is the ohmic resistance of the electrolyte, l is the distance between the two electrodes and S is the area of the electrodes. And the values were summarized in Table 3. The data generally reveal conductivities in the range 1×10^{-4} S/cm for all ionic crystals based electrolytes examined. The conductivities of $[C_nBEP][BF_4]_2$ (n = 4, 5, 6, 8) based electrolytes rank in terms of alkyl chain length: 6 > 8 > 5 > 4. The ion conductivities increase from 1.39×10^{-4} S/cm to 2.92×10^{-4} S/cm when the value of n increase from 4 to 6, and then decrease to 1.99×10^{-4} S/cm as n is equal to 8. The similar trend was observed in the benzothiaozole-based dicationic conductors that we synthesized previously.[29] We suppose that this tendency is closely associated with the ion-conductive channel in the electrolyte

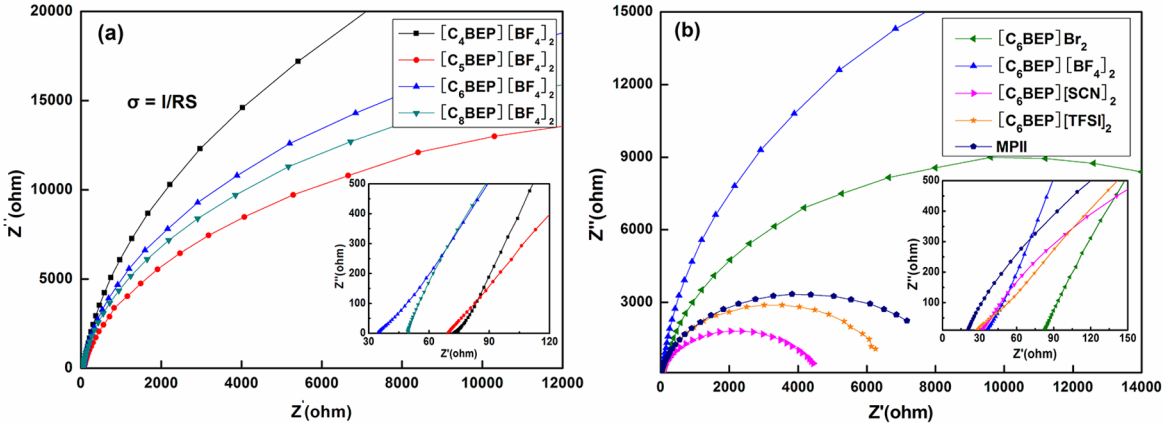

Figure 5. Nyquist plots for (a) $[C_nBEP][BF_4]_2$ (n = 4, 5, 6, 8) and (b) $[C_6BEP][X]_2$ (X = BF_4, Br, TFSI, SCN) and MPII-based electrolyts.

DOI: 10.1021/acsami.5b06035
ACS Appl. Mater. Interfaces 2015, 7, 21381−21390

Table 3. Ionic Conductivities and D_{app} (I_3^-) of the Ionic Crystal-Based Electrolytes

electrolyte	conductivity ($\times 10^{-4}$ S/cm)	I_{ss} (I^-) ($\times 10^{-7}$ A)	D_{app} (I^-) ($\times 10^{-7}$ cm^2/s)	I_{ss} (I_3^-) ($\times 10^{-7}$ A)	D_{app} (I_3^-) ($\times 10^{-6}$ cm^2/s)
$[C_4BEP][BF_4]_2$	1.39	0.134	0.477	0.617	0.879
$[C_5BEP][BF_4]_2$	1.45	0.161	0.574	0.676	0.963
$[C_6BEP][BF_4]_2$	2.92	0.716	2.551	0.941	1.341
$[C_8BEP][BF_4]_2$	1.99	0.290	1.033	0.887	1.264
$[C_6BEP][Br]_2$	1.23	0.262	0.933	0.819	1.167
$[C_6BEP][TFSI]_2$	3.98	1.524	5.430	2.564	3.654
$[C_6BEP][SCN]_2$	3.42	1.336	4.760	1.656	2.360
MPII	5.03	0.469	1.671	1.729	2.464

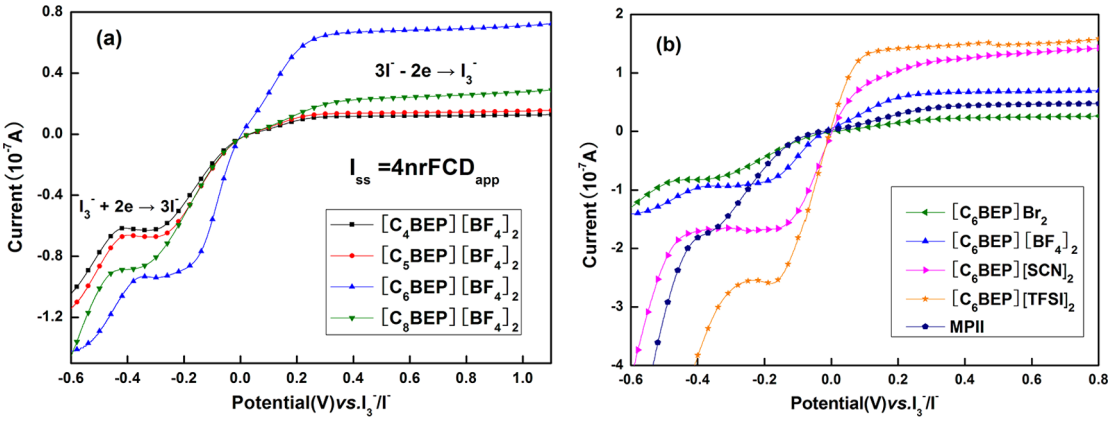

Figure 6. Steady-state voltammograms of (a) $[C_nBEP][BF_4]_2$ (n = 4, 5, 6, 8) and (b) $[C_6BEP][X]_2$ (X = BF_4, Br, TFSI, SCN) and MPII-based electrolyts.

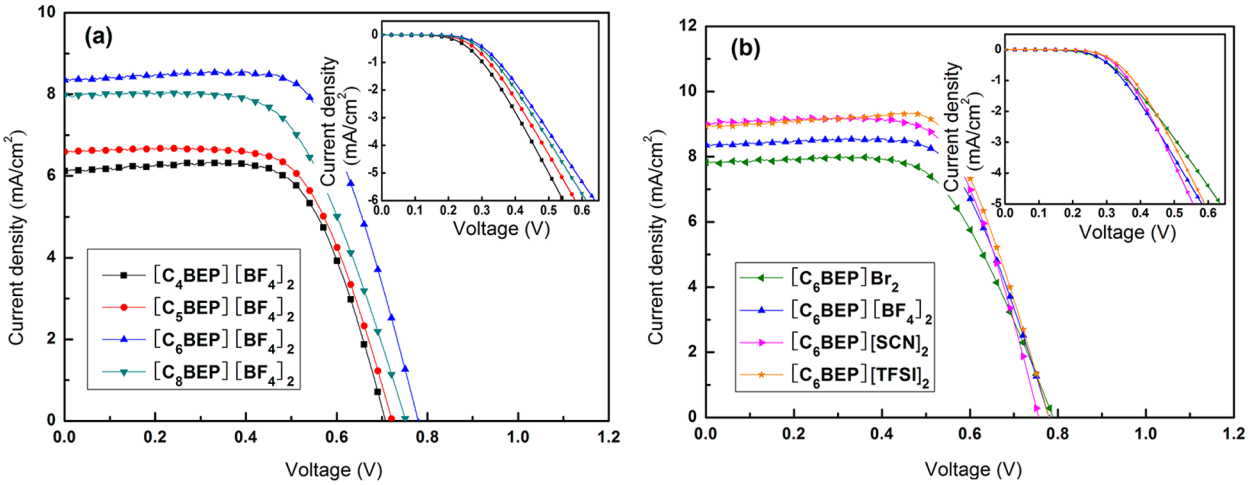

Figure 7. J–V curves of devices based on the electrolytes using (a) $[C_nBEP][BF_4]_2$ (n = 4, 5, 6, 8) as matrixes and (b) $[C_6BEP][X]_2$ (X = BF_4, Br, TFSI, SCN) as matrixes under 1.5 sun light intensity illumination and in dark conditions. Inset: under dark conditions.

because of the relatively suitable saturated carbon chain and the ion-conductivity layer number per unit length.[29] The anion species of crystals greatly affect the conductivity. $[C_6BEP][TFSI]_2$ based electrolyte displays the highest room temperature conductivity, 3.98×10^{-4} S/cm, which is a third higher than that of $[C_6BEP][BF_4]_2$ based one. $[C_6BEP][SCN]_2$-based electrolyte closely follows; the electrolyte with the lowest conductivity is $[C_6BEP]$ $[Br]_2$. The above data demonstrate both the alkylene chain and the anion in dicationic crystals have significant influence on the electrochemical property of this kind of compounds.

Regeneration of dye sensitizer molecules by reducing species contained in the electrolyte is a key mechanism in DSSC device because it competes kinetically with a detrimental charge recombination process.[33] If triiodide ion does not diffuse fast enough, it will have an influence on the dye regeneration, which results to the lower performance of device.[34] Hence it is necessary to characterize the influence of ionic crystal structure on the apparent diffusion coefficients of triiodide/iodide, D_{app} (I_3^-)/D_{app} (I^-). In our experiment, D_{app} (I_3^-)/D_{app} (I^-) of $[C_nBEP][BF_4]_2$ (n = 4, 5, 6, 8) and $[C_6BEP][X]_2$ (X = Br, TFSI, SCN) were determined by the steady-state voltammograms (as shown in Figure 6). The values were calculated according to the equation inserted in Figure 6a, where n is the number of electrons per molecule, F is the Faraday constant, C is the concentration, and r is the radius of the electrode. And

DOI: 10.1021/acsami.5b06035
ACS Appl. Mater. Interfaces 2015, 7, 21381−21390

the calculated values were summarized in Table 3. The changing trends in D_{app} of the I^-/I_3^- redox couple are similar to that of the ion conductivity, and the $[C_6BEP][TFSI]_2$ based electrolyte shows the highest D_{app} (I_3^-) of 3.654×10^{-6} cm^2/s, which is significantly higher than that of $[C_6BEP][BF_4]_2$-based electrolyte. To illustrate the role of ionic crystal matrix, we substituted the crystal matrix to the ionic liquid with high conductivity, MPII,[35,36] and measured the relational parameters (as shown in Table 3). The diffusion coefficients of triiodide ion for $[C_6BEP][TFSI]_2$ and MPII are 3.654×10^{-6} cm^2/s and 2.464×10^{-6} cm^2/s, respectively. The superior D_{app} (I_3^-) of $[C_6BEP][TFSI]_2$ indicates that the crystal structure with three-dimensional channel is beneficial to the ion diffusion.

Photocurrent–Density–Voltage Characteristics of DSSCs. To further investigate the ionic crystal-based electrolytes, they have been incorporated into DSSCs devices in combination with the N719 dye, and photovoltaic performance was performed under AM 1.5 illumination as shown in Figure 7. The detailed parameters are given in Table 4. Figure 7 shows

Table 4. Device Performances of DSSCs with Different Electrolytes

electrolytes	J_{sc} (mA/cm^2)	V_{oc} (V)	FF (%)	PCE (%)
$[C_4BEP][BF_4]_2$/DMPII/I_2	6.2	0.71	66.79	2.94
$[C_5BEP][BF_4]_2$/DMPII/I_2	6.58	0.72	66.70	3.16
$[C_6BEP][BF_4]_2$/DMPII/I_2	8.39	0.78	66.62	4.36
$[C_8BEP][BF_4]_2$/DMPII/I_2	7.95	0.75	61.22	3.65
$[C_6BEP][Br]_2$/DMPII/I_2	7.84	0.79	61.19	3.79
$[C_6BEP][SCN]_2$/DMPII/I_2	9.05	0.76	66.30	4.56
$[C_6BEP][TFSI]_2$/DMPII/I_2	8.98	0.78	68.10	4.77
$[C_6BEP][TFSI]_2$/EMII/I_2	12.04	0.76	64.26	5.88
$[C_6BEP][TFSI]_2$/MPII/I_2	12.35	0.75	60.13	5.57
$[C_6BEP][TFSI]_2$/DMPII/MPII/I_2	12.33	0.81	60.28	6.02

the photocurrent density-photovoltage (J–V) curves of DSSCs using $[C_nBEP][BF_4]_2$ (n = 4, 5, 6, 8) and $[C_6BEP]X_2$ (X = Br, TFSI, SCN) based electrolytes under AM 1.5 sun illumination and in dark condition. In the serials of $[C_nBEP][BF_4]_2$ (n = 4, 5, 6, 8) based electrolytes, the DSSC employing $[C_6BEP][BF_4]_2$ gives a short-circuit photocurrent density of 8.39 mA/cm^2, open-circuit voltage of 0.78 V, and PCE of 4.36%. These parameters were clearly lower than those for the DSSC prepared with $[C_6BEP][TFSI]_2$ (J_{sc} = 8.98 mA/cm^2, V_{oc} = 0.78 V, and PCE = 4.77%). Higher J_{sc} benefits from better ionic conductivity and larger ionic diffusion coefficients.[14,37]

The raise found for the value of V_{oc} in $[C_6BEP][TFSI]_2$-based electrolyte could be ascribed to the remarkably higher D_{app} (I_3^-) and conductivity of the electrolyte with the $[C_6BEP][TFSI]_2$. The value of V_{oc} for DSSC with I^-/I_3^- redox electrolyte can be represented by the following equation[38]

$$V_{oc} = \frac{kT}{e}\ln\left(\frac{I_{inj}}{n_{cb}k_{et}[I_3^-]}\right) \quad (1)$$

where k and T are the Boltzmann constant and absolute temperature, respectively, I_{inj} is the injection current from dye to semiconductor, n_{cb} is the electron density on the conduction band of the semiconductor, and k_{et} is the rate constant for I_3^- reduction. According to the eq 1, the higher V_{oc} of the $[C_6BEP][TFSI]_2$-based electrolyte is related to the suppression of the dark current at the TiO_2 electrode/electrolyte interface.[39] The dark current originates from the reduction of triiodide by conduction band electrons from TiO_2.[40] At the interface of the dye-sensitized TiO_2 photoanode and electrolyte, a higher diffusion coefficient of triiodide can promote the transport of triiodide to the Pt counter electrode for the iodide form, thus ensuring a lower triiodide reduction rate (k_{et}) and a higher V_{oc}.[41] As shown in Figure 7a, the onset of dark current has a positive shift of about 200 mV from the $[C_6BET][BF_4]_2$-based electrolyte to $[C_6BEP][TFSI]_2$-based electrolyte. As mentioned above, the drop of dark current is attributed to the higher triiodide diffusion coefficient in the $[C_5MBT][TFSI]_2$-based electrolyte.

Besides investigating the influence of ionic crystal on the performance of cell, the effect of I^- source was also checked by fabricating the $[C_6BEP][TFSI]_2$ based DSSCs with different I^- source, such as EMII, MPII, and MPII/DMPII, as shown in Figure 8 and Table 4. When using the mixture of DMPII and

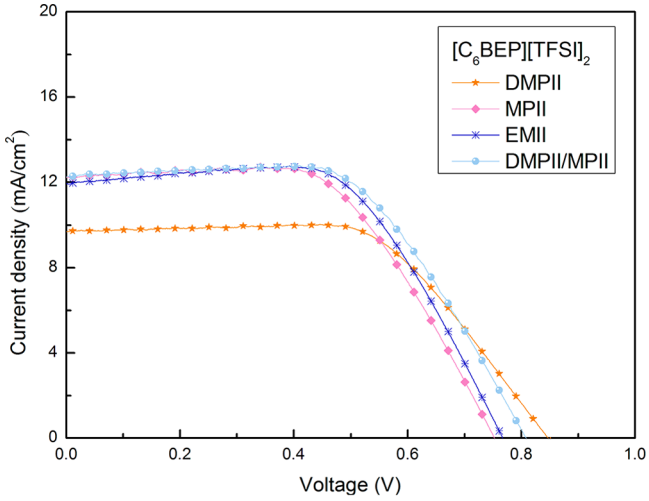

Figure 8. J–V curves of $[C_6BEP][TFSI]_2$ based devices with different I^- source under 1.5 sun light intensity illumination.

MPII as I^- source (the molar proportion of DMPII/MPII = 0.05:0.05), the all-solid-state DSSC device produced a J_{sc} of 12.33 mA/cm^2, a V_{oc} of 0.81 V, and an FF of 60.28%, corresponding to a PCE of 6.02%. The superior efficiency can be attributed to the significant raise of J_{sc}, increasing by 2.56 mA/cm^2 compared with that of device using DMPII as I^- source.

From Table 4, it is worthwhile to note that the change of values of J_{sc} is most notable than other photovoltaic parameters as the changes of length of alkylene chain and anion, from the minimum of 6.2 mA/cm^2 ($[C_4BEP][BF_4]_2$/DMPII/I_2 based device) to maximum of 12.33 mA/cm^2 roughly doubled ($[C_6BEP][TFSI]_2$/DMPII/MPII/I_2-based device). This can be ascribed to enhanced triiodide diffusion coefficient. Photocurrent collection strongly depends on the speed of charge transport in the electrolyte, and the concentration of triiodide is much lower than that of iodide which is diffuses faster than the former in practical electrolytes.[42,44] Hence, the overall charge transport is determined by the motion of triiodide. To address this, we measured the D_{app} (I_3^-) of $[C_6BEP][TFSI]_2$-based electrolytes with different I^- sources (as shown in Table 5). The cell based on $[C_6BEP][TFSI]_2$/DMPII/MPII/I_2 electrolyte with the highest efficiency of 6.02%

DOI: 10.1021/acsami.5b06035
ACS Appl. Mater. Interfaces 2015, 7, 21381–21390

Table 5. D_{app} (I_3^-) of $[C_6BEP][TFSI]_2$-Based Electrolytes with Different I^- Sources

I^- source	I_{ss} (I^-) ($\times 10^{-7}$ A)	D_{app} (I^-) ($\times 10^{-7}$ cm^2/s)	I_{ss} (I_3^-) ($\times 10^{-7}$ A)	D_{app} (I_3^-) ($\times 10^{-6}$ cm^2/s)
DMPII	1.524	5.430	2,564	3.654
DMPII/MPII	1.359	4.842	3.285	4.681

shows the highest D_{app} (I_3^-) of 4.681 $\times$ 10^{-6} cm^2/s for five times that of the device with $[C_4BEP][BF_4]_2$/DMPII/I_2. Thus, the trend of J_{sc} in DSSCs matches well with the results of D_{app} (I_3^-) in electrolytes.

Electrochemical Impedance Spectra of DSSCs. Electrochemical impedance spectroscopy (EIS) measurements have been utilized to describe the effect on the $J-V$ characteristics of several interfacial charge-transfer and transport mechanisms occurring in DSSC.[43] We addressed the impedance spectroscopy of devices using the different pyrrolidinium based ionic crystals as matrixes for electrolytes, as shown in Figure 9. And Table 6 presents the parameters of the cells measured. At applied potentials, typical impedance spectra of a dye-sensitized solar cell show three arcs in Nyquist plot.[44] The main contribution to the high-frequency semicircle arises from the parallel connection of C_{pt} and R_{pt}, which is the charge-transfer resistance at the counter electrode/electrolyte interface.[45] The intermediate-frequency is the combination of C_μ and R_r, which is a charge-transfer resistance related to recombination of electrons at the TiO_2/electrolyte interface.[45] The low-frequency corresponds to R_d, which is the charge-transfer resistance concerned with the diffusion of I_3^- in the electrolyte. Furthermore, there is the other resistance in cell, R_s, which is a series resistance accounting for the transport resistance of the TCO. The resistance given by the sum of R_{pt}, R_r, R_d, and R_s, is the total resistance of device. Within a very good approximation, this impedance spectrum may be modeled by the equivalent circuit inserted in Figure 9a.

Table 6. Parameters Obtained by the EIS of the Devices Fabricated with Different Electrolytes

electrolyte	R_s (Ω)	R_r (Ω)	R_{pt} (Ω)	f_{max} (Hz)	τ_e (ms)
$[C_4BEP][BF_4]_2$/DMPII/I_2	53.3	62.28	49.72	19.456	8.180
$[C_5BEP][BF_4]_2$/DMPII/I_2	44.1	64.01	42.93	19.056	8.352
$[C_6BEP][BF_4]_2$/DMPII/I_2	34.2	60.43	17.19	18.858	8.440
$[C_8BEP][BF_4]_2$/DMPII/I_2	39.2	62.81	28.57	18.984	8.384
$[C_6BEP][Br]_2$/DMPII/I_2	48.4	78.05	23.86	22.541	7.061
$[C_6BEP][SCN]_2$/DMPII/I_2	24.4	52.74	17.62	18.598	8.558
$[C_6BEP][TFSI]_2$/DMPII/I_2	21.3	73.17	11.98	5.883	27.053
$[C_6BEP][TFSI]_2$/DMPII/MPII/I_2	22.3	85.91	13.82	2.556	62.267

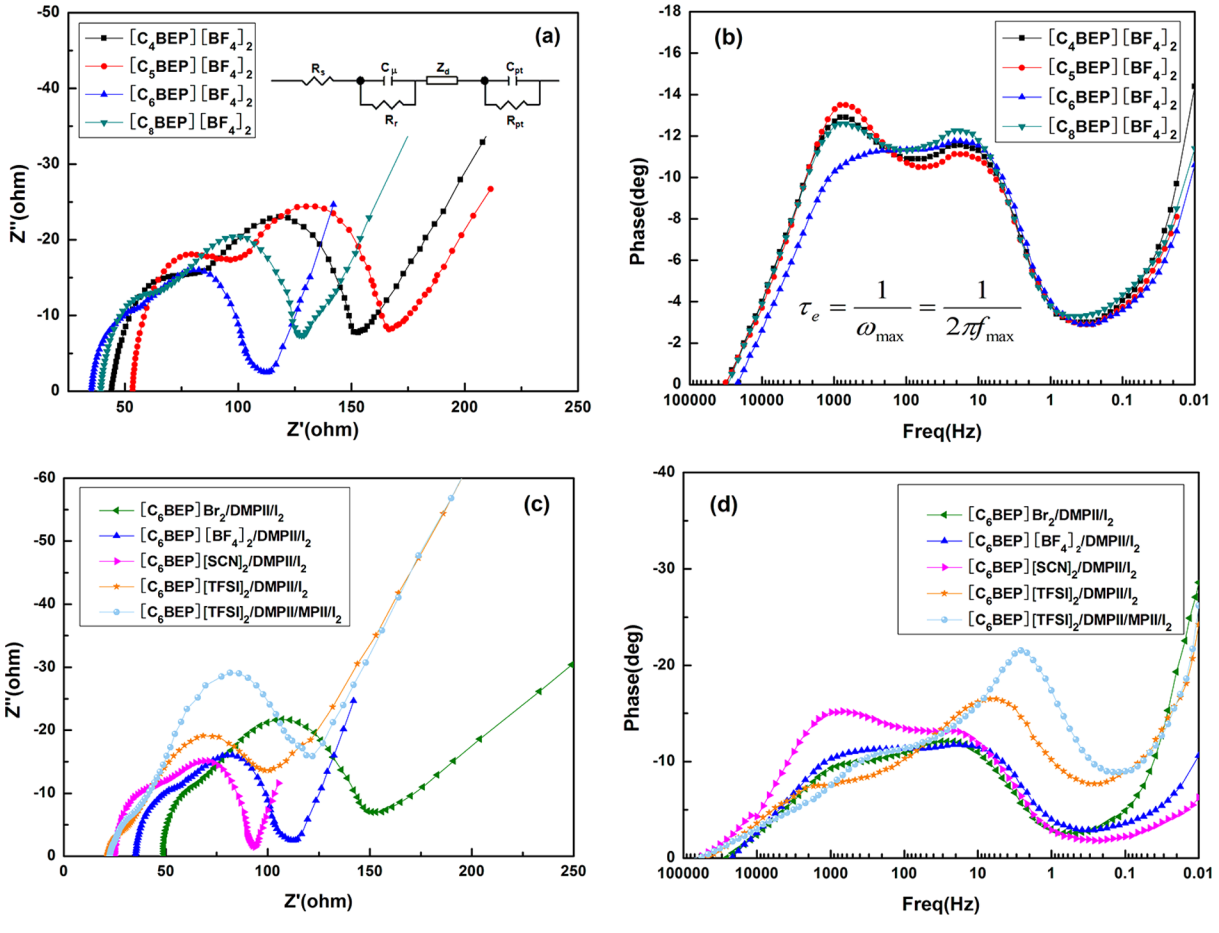

Figure 9. (a) Nyquist plots and (b) fitted Bode phase plots of the devices with $[C_nBEP][BF_4]_2$ (n = 3, 4, 5, 6) based electrolytes under dark condition; (c) Nyquist plots and (d) fitted Bode phase plots of the devices with $[C_6BEP][X]_2$ (X = BF_4, Br, TFSI, SCN) and different I^- source-based electrolytes under dark conditions.

DOI: 10.1021/acsami.5b06035
ACS Appl. Mater. Interfaces 2015, 7, 21381−21390

Table 6 shows the value of R_r in DSSC with $[C_6BEP][TFSI]_2$ is 73.17 Ω, which is superior to other those in the series of DSSCs with $[C_nBEP][X]_2$ (n = 3, 4, 5, 6) (X = BF_4, Br, TFSI, SCN). It indicates that the electron recombination can be effectively inhibited in device with $[C_6BEP][TFSI]_2$, which agrees quite well with the results of dark current (Figure 7b). As using the mixture of DMPII/MPII as I^- source, the value of R_r has a further increase, reaching to 85.9 Ω, which makes this cell with the lower rate constant for I_3^- reduction (k_{et}) and further leads to the higher V_{oc} (0.81 V) compared with that of device with $[C_6BEP][TFSI]_2$/DMPII (0.78 V).

Contrary to the changing trend of the values of R_r, the values of R_s approximately tail off in the series of DSSCs with $[C_nBEP][X]_2$ (n = 3, 4, 5, 6) (X = BF_4, Br, TFSI, SCN) until the device with $[C_6BEP][TFSI]_2$ shows the lowest value, 21.3 Ω (Table 6). This low value of R_s contributes to the favorable fill factor (FF) and high overall efficiency in device with $[C_6BEP][TFSI]_2$.[43]

Comparing with the values of R_r and R_s, those of R_{pt} show obvious difference in devices with $[C_nBEP][X]_2$ (n = 3, 4, 5, 6) (X = BF_4, Br, TFSI, SCN). In DSSC with $[C_6BEP][TFSI]_2$, 11.98 Ω of the value of R_{pt} is only one-quarter of that of device with $[C_4BEP][BF_4]_2$. As pointed out above, R_{pt} is associated with the charge transfer at electrolyte/Pt-FTO interface, $I_3^- \rightarrow I^-$, of which the smaller value implies the easy of reduction of triiodide. Therefore, apart from R_r and R_s, the low value of R_{pt} mainly facilitates the device with $[C_6BEP][TFSI]_2$ to show high efficiency. The lowest value of R_{pt} may be explained by the good interfacial compatibility of electrolyte with Pt counter electrode. We tried to illustrate the penetration of the electrolyte on Pt electrode by FESEM photograph of the cross-section views, but we failed because the layer of $PtCl_4$ is too thin to be characterized. Then we employed cyclic voltammetry (CV) to determine the interfacial compatibility of electrolyte, using symmetrical Pt electrode sandwiched with ionic crystal-based electrolyte (as shown in Figure 10). $[C_6BEP][TFSI]_2$/DMPII and $[C_6BEP][TFSI]_2$/DMPII/MPII based electrolytes have the peak current densities of 16.51 mA/cm^2 and 16.71 mA/cm^2 respectively, which are higher than the values for other electrolytes. It confirms that the Pt counter electrodes show remarkably catalytic activity for $[C_6BEP][TFSI]_2$ based cells which favor the reduction of I_3^- to I^-. This result is in good agreement with the parameters obtained by EIS.

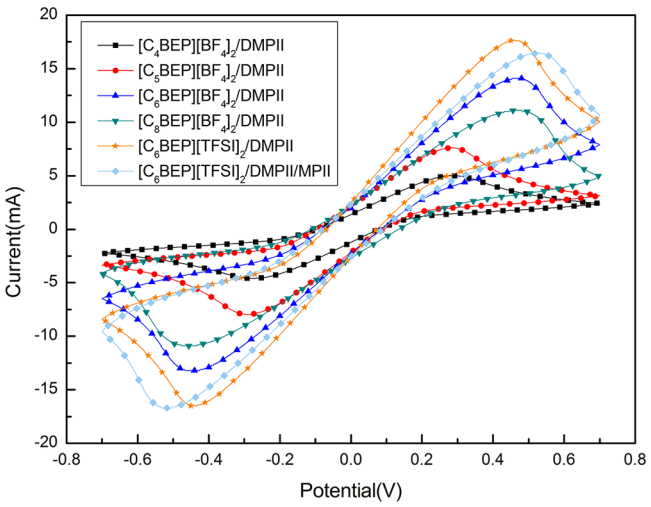

Figure 10. Cyclic voltammetry spectra of ionic crystal-based electrolytes.

The effective lifetime of the electron (τ_e) before recombination in the dye-sensitized TiO_2 electrode is a important parameter to discuss the performance of cell. And the values were calculated according to the equation inserted in Figure 9b, where f_{max} is the maximum frequency of the midfrequency peak of the Bode phase plot.[46] The f_{max} and the electron lifetime were also summarized in Table 6. As we can see, the devices with $[C_nBEP][BF_4]_2$ (n = 4, 5, 6, 8) show the electron lifetimes from 8.180 to 8.440 ms, remaining nearly unchanged. However, the anion change from BF_4^- to $TFSI^-$ for $[C_6BEP][X]_2$ crystals makes the electron lifetime increase more than three times, which indicates that the anion has more significant influence on the value of τ_e than the length of alkylene chain in crystal. When changing I^- source to the mixture of DMPII/MPII, the value of τ_e is affected more, rising to nearly eight times, which is one of the reasons that photovoltaic performance of this cell is superior to those of other cells. Taking into account that the electron lifetime is the product of R_r and C_μ, $\tau_e = R_rC_\mu$, we think that the longer electron lifetime may be introduced by the higher value of R_r in the cell with $[C_6BEP][TFSI]_2$/DMPII/MPII.

IPCE of DSSC. The incident photon to current conversion efficiency (IPCE) of the device based on $[C_6BEP][TFSI]_2$/DMPII/MPII is shown as an example in Figure 11. It exhibits a maximum of 51% at 530 nm is reached for the electrolyte.

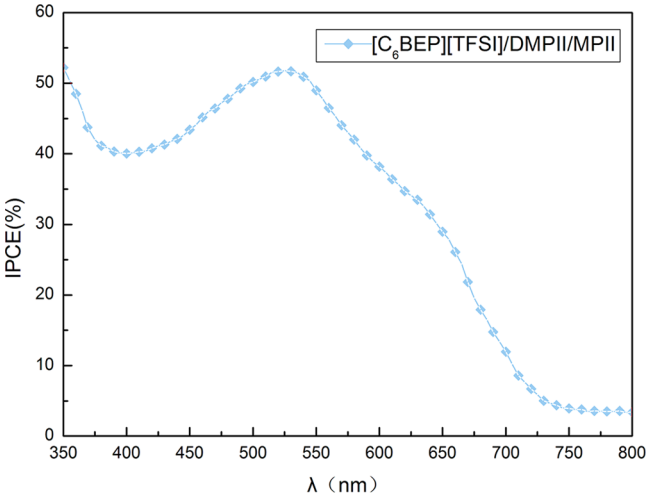

Figure 11. Incident photon to current conversion efficiency of the device based on $[C_6BEP][TFSI]_2$/DMPII/MPII.

Long-Term Stability of DSSC. After successfully testing the photoelectric performances of DSSCs, the long-term stability of the device based on the solid electrolyte with $[C_6BEP][TFSI]_2$/DMPII/MPII was recorded over a period of 960 h (as shown in Figure 12 and Figure S15 in Supporting Information), and the data were summarized in Table S1 in Supporting Information. As compared to the initial performance parameter, there are the drops of 0.99 mA/cm^2 and 0.04 V in the values of J_{sc} and V_{oc} after 960 h, respectively. The device retained approximately 92% of the initial efficiency after 960 h, confirming the very high stability of the device.

DOI: 10.1021/acsami.5b06035
ACS Appl. Mater. Interfaces 2015, 7, 21381−21390

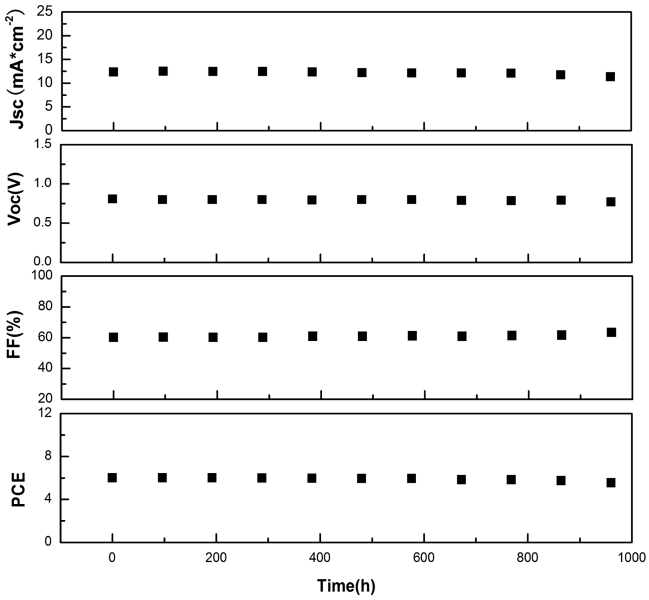

Figure 12. Evolution of the photovoltaic parameters of device with $[C_6BEP][TFSI]_2$/DMPII/MPII during 960 h.

CONCLUSION

Using pyrrolydinium-based ionic crystal as matrix has led to the discovery of new solid-state electrolyte for DSSC. The microstructure with three-dimensional ionic channels in this kind of ionic crystals makes ionic crystals with good conductivity and diffusion efficiency, and then ensures the high efficiency and excellent stability. An efficiency of 6.02% have achieved in full sunlight on the optimized condition. By studying the influence of crystal structure on the electrochemical properties and device performances, we found that the length of the linkage chain separating the geminal dication and the nature of anion have the marked impact on the electrochemical properties of ionic crystal, therefore influence the performance of device. We believe that our findings on dicationic crystals will provide useful clues for further improvement of solid-state electrolytes.

ASSOCIATED CONTENT

Supporting Information

The Supporting Information is available free of charge on the ACS Publications website at DOI: 10.1021/acsami.5b06035.

Figures S1−S15 and Table S1 (PDF)

AUTHOR INFORMATION

Corresponding Authors

*E-mail: wangyefeng@snnu.edu.cn.
*E-mail: jhzeng@ustc.edu.

Notes

The authors declare no competing financial interest.

ACKNOWLEDGMENTS

This work was supported by the Natural Science Foundation of China (No. 21071093), and Fundamental Research Funds for the Central Universities (Grants GK201503032, GK201402017, GK201101004) from the Department of Education (DoE).

REFERENCES

(1) Su'ait, M. S.; Rahman, M. Y. A.; Ahmad, A. Review on Polymer Electrolyte in Dye-Sensitized Solar Cells (DSSCs). *Sol. Energy* **2015**, *115*, 452−470.
(2) Mathew, S.; Yella, A.; Gao, P.; Humphry-Baker, R.; Curchod, B. F. E.; Ashari-Astani, N.; Tavernelli, I.; Rothlisberger, U.; Nazeeruddin, M. K.; Grätzel, M. Dye-Sensitized Solar Cells with 13% Efficiency Achieved Through the Molecular Engineering of Porphrin Sensitizers. *Nat. Chem.* **2014**, *6*, 242−247.
(3) Li, D.; Qin, D.; Deng, M.; Luo, Y.; Meng, Q. Optimization the Solid-State Electrolytes for Dye-Sensitized Solar Cells. *Energy Environ. Sci.* **2009**, *2*, 283−291.
(4) Wu, J.; Hao, S.; Lan, Z.; Lin, J.; Huang, M.; Huang, Y.; Fang, L.; Yin, S.; Sato, T. A Thermoplastic Gel Electrolyte for Stable Quasi-Solid-State Dye-Sensitized Solar Cells. *Adv. Funct. Mater.* **2007**, *17*, 2645−2652.
(5) Brennan, L. J.; Barwich, S. T.; Satti, A.; Faure, A.; Gunko, Y. K. Graphene-Ionic Liquid Electrolytes for Dye Sensitized Solar Cells. *J. Mater. Chem. A* **2013**, *1*, 8379−8384.
(6) Etgar, L.; Schuchardt, G.; Costenaro, D.; Carniato, F.; Bisio, C.; Zakeeruddin, S. M.; Nazeeruddin, M. K.; Marchese, L.; Grätzel, M. Enhancing the Open Circuit Voltage of Dye Sensitized Solar Cells by Surface Engineering of Silica Particles in A Gel Electrolyte. *J. Mater. Chem. A* **2013**, *1*, 10142−10147.
(7) Kumara, R. A.; Konno, A.; Shiratsuchi, K.; Tsukahara, J.; Tennakone, K. Dye-Sensitized Solid-State Solar Cells: Use of Crystal Growth Inhibitors for Deposition of the Hole Collector. *Chem. Mater.* **2002**, *14*, 954−955.
(8) Bach, U.; Comte, P.; Moser, J. E.; Weissortel, F.; Salbeck, J.; Spreitzer, H.; Grätzel, M. Solid-State Dye-Sensitized Mesoporous TiO_2 Solar Cells with High Photon-to-Electron Conversion Efficiencies. *Nature* **1998**, *395*, 583−585.
(9) Wu, J.; Lan, Z.; Lin, J.; Huang, M.; Huang, Y.; Fan, L.; Luo, G. Electrolytes in Dye-Sensitized Solar Cells. *Chem. Rev.* **2015**, *115*, 2136−2173.
(10) Chen, X.; Zhao, J.; Zhang, J.; Qiu, L.; Xu, D.; Zhang, H.; Han, X.; Sun, B.; Fu, G.; Zhang, Y.; Yan, F. Bis-Imidazolium Based Poly(ionic liquid) Electrolytes for Quasi-Solid-State Dye-Sensitized Solar Cells. *J. Mater. Chem.* **2012**, *22*, 18018−18024.
(11) Harikisun, R.; Desilvestro, H. Long-Term Stability of Dye Solar Cells. *Sol. Energy* **2011**, *85*, 1179−1188.
(12) Cao-Cen, H.; Zhao, J.; Qiu, L.; Xu, D.; Li, Q.; Chen, X.; Yan, F. High Performance All-Solid-State Dye-Sensitized Solar Cells Based on Cyanobiphenyl-Functionalized Imidazolium-Type Ionic Crystals. *J. Mater. Chem.* **2012**, *22*, 12842−12850.
(13) MacFarlane, D. R.; Tachikawa, N.; Forsyth, M.; Pringle, J. M.; Howlett, P. C.; Elliott, G. D.; Davis, J. H., Jr; Watanabe, M.; Simon, P.; Angell, C. A. Energy Application of Ionic Liquids. *Energy Environ. Sci.* **2014**, *7*, 232−250.
(14) Wang, H.; Li, J.; Gong, F.; Zhou, G.; Wang, Z. S. Ionic Conductor with High Conductivity as Single-Component Electrolyte for Efficient Solid-State Dye-Sensitized Solar Cells. *J. Am. Chem. Soc.* **2013**, *135*, 12627−12633.
(15) Zhao, Y.; Zhai, J.; He, J.; Chen, X.; Chen, L.; Zhang, L.; Tian, Y.; Jiang, L.; Zhu, D. High-Performance All-Solid-State Dye-Sensitized Solar Cells Utilizing Imidazolium-Type Ionic Crystal as Charge Transfer Layer. *Chem. Mater.* **2008**, *20*, 6022−6028.
(16) Midya, A.; Xie, Z.; Yang, J.; Chen, Z.; Blackwood, D.; Wang, J.; Adams, S.; Loh, K. P. A New Class of Solid State Ionic Conductors for Application in All Solid State Dye Sensitized Solar Cells. *Chem. Commun.* **2010**, *46*, 2091−2093.
(17) Wang, H.; Zhang, X.; Gong, F.; Zhou, G.; Wang, Z. S. Novel Ester-Functionalized Solid-State Electrolyte for Highly Efficient All-Solid-State Dye-Sensitized Solar Cells. *Adv. Mater.* **2012**, *24*, 121−124.
(18) Li, J.; Wang, H.; Zhou, G.; Wang, Z. S. Hydroxyethyl and Ester Co-Functionalized Imidazolium Iodide for Highly Efficient Solid-State Dye-Sensitized Solar Cells. *Chem. Commun.* **2013**, *49*, 9446−9448.
(19) Xu, X.; Wang, H.; Gong, F.; Zhou, G.; Wang, Z. S. Performance Enhancement of Dye-Sensitized Solar Cells Using an Ester-Function-

DOI: 10.1021/acsami.5b06035
ACS Appl. Mater. Interfaces 2015, 7, 21381−21390

alized Imidazolium Iodide as the Solid State Electrolyte. *ACS Appl. Mater. Interfaces* **2013**, *5*, 3219−3223.
(20) Li, J.; Lv, K.; Sun, H.; Wang, Z. S. Effect of Substituents in the Imidazolium Ring on the Performance of Solid-State Dye-Sensitized Solar Cells. *Nano* **2014**, *9*, 1440006.
(21) Döbbelin, M.; Azcune, I.; Bedu, M.; Ruiz de Luzuriaga, A.; Genua, A.; Jovanovski, V.; Cabañero, G.; Odriozola, I. Synthesis of Pyrrolidinium-Based Poly(ionic liquid) Electrolytes with Poly(ethylene glycol) Side Chains. *Chem. Mater.* **2012**, *24*, 1583−1590.
(22) Zhou, Q.; Boyle, P. D.; Malpezzi, L.; Mele, A.; Shin, J. H.; Passerini, S.; Henderson, W. A. Phase Behavior of Ionic Liquid-LiX Mixtures: Pyrrolidinium Cations and $TFSI^-$ Anions-Linking Structure to Transport Properties. *Chem. Mater.* **2011**, *23*, 4331−4337.
(23) Yoon, H.; Lane, G. H.; Shekibi, Y.; Howlett, P. C.; Forsyth, M.; Best, A. S.; MacFarlane, D. R. Lithium Electrochemistry and Cycling Behaviour of Ionic Liquids Using Cyano Based anions. *Energy Environ. Sci.* **2013**, *6*, 979−986.
(24) MacFarlane, D. R.; Huang, J. H.; Forsyth, M. Lithium-Doped Plastic Crystal Electrolytes Exhibiting Fast Ion Conduction for Secondary Batteries. *Nature* **1999**, *402*, 792−794.
(25) Jovanovski, V.; González-Pedro, V.; Giménez, S.; Azaceta, E.; Cabañero, G.; Grande, H.; Tena-Zaera, R.; Mora-Seró, I.; Juan Bisquert, J. A Sulfide/Polysulfide-Based Ionic Liquid Electrolyte for Quantum Dot-Sensitized Solar Cells. *J. Am. Chem. Soc.* **2011**, *133*, 20156−20159.
(26) Armel, V.; Forsyth, M.; MacFarlane, D. R.; Pringle, J. M. Organic Ionic Plastic Crystal Electrolytes; A New Class of Electrolyte for High Efficiency Solid State Dye-Sensitized Solar Cells. *Energy Environ. Sci.* **2011**, *4*, 2234−2239.
(27) Li, Q.; Chen, X.; Zhao, J.; Qiu, L.; Zhang, Y.; Sun, B.; Yaan, F. Organic Ionic Plastic Crystal-Based Electrolytes for Solid-State Dye-Sensitized Solar Cells. *J. Mater. Chem.* **2012**, *22*, 6674−6679.
(28) Li, Q.; Zhao, J.; Sun, B.; Lin, B.; Qiu, L.; Zhang, Y.; Chen, X.; Lu, J.; Yan, F. High-Temperature Solid-State Dye-Sensitized Solar Cells Based on Organic Ionic Plastic Crystal Electrolytes. *Adv. Mater.* **2012**, *24*, 945−950.
(29) Han, L.; Wang, Y. F.; Zeng, J. H. Effective Solid Electrolyte Based on Benzothiazolium for Dye-Sensitized Solar Cells. *ACS Appl. Mater. Interfaces* **2014**, *6*, 22088−22095.
(30) Alunni, S.; Tijskens, P. Study on the Effect of the Structure of the Leaving Group in the Elcb Mechanism of Base-Promoted *β*-Elimination Reactions from N-[2-(*p*-Nitrophenyl)ethyl]-alkylammonium Ions. *J. Org. Chem.* **1995**, *60*, 8371−8374.
(31) Anderson, J. L.; Ding, R.; Ellern, A.; Armstrong, D. W. Structure and Properties of High Stability Geminal Dicationic Ionic Liquids. *J. Am. Chem. Soc.* **2005**, *127*, 593−604.
(32) Lee, M.; Niu, Z.; Slebodnick, C.; Gibson, H. W. Structure and Properties of *N,N*-Alkylene Bis(*N*′-Alkylimidazolium) Salts. *J. Phys. Chem. B* **2010**, *114*, 7312−7319.
(33) Teuscher, J.; Marchioro, A.; Andrès, J.; Roch, L. M.; Xu, M.; Zakeeruddin, S. M.; Wang, P.; Grätzel, M.; Moser, J. Kinetics of the Regeneration by Iodide of Dye Sensitizers Adsorbed on Mesoporous Titania. *J. Phys. Chem. C* **2014**, *118*, 17108−17115.
(34) Wyss, P.; Moehl, T.; Zakeeruddin, S. M.; Grätzel, M. Influence of Cations of the Electrolyte on the Performance and Stability of Dye Sensitized Solar Cells. *J. Mater. Chem.* **2012**, *22*, 24424−24429.
(35) Wang, P.; Zakeeruddin, S.; Exanr, I.; Grätzel, M. High Efficiency Dye-Sensitized Nanocrystalline Solar Cells Based on Ionic Liquid Polymer Gel Electrolyte. *Chem. Commun.* **2002**, 2972−2973.
(36) Pan, X.; Dai, S. Y.; Wang, K. J. New Type High Efficient Quasi-Solid-State Ionic Liquid Electrolyte for Dye-Sensitized Solar Cells. *Chin. J. Chem.* **2007**, *25*, 1601−1603.
(37) Li, S. C.; Qiu, H. C.; Shi, C. Z.; Chen, X. J.; Yan, F. Water-Resistant, Solid-State, Dye-Sensitized Solar Cells Based on Hydrophobic Organic Ionic Plastic Crystal Electrolytes. *Adv. Mater.* **2014**, *26*, 1266−1271.
(38) Hagfeldt, A.; Grätzel, M. Light-Induced Redox Reactions in Nanocrystalline Systems. *Chem. Rev.* **1995**, *95*, 49−68.
(39) Wang, P.; Zakeeruddin, S. M.; Comte, P.; Charvet, R.; Humphry-Baker, R.; Grätzel, M. Enhance the Performance of Dye-Sensitized Solar Cells by Co-grafting Amphiphilic Sensitizer and Hexadecylmalonic Acid on TiO_2 Nanocrystals. *J. Phys. Chem. B* **2003**, *107*, 14336−14341.
(40) Nazeeruddin, M. K.; Kay, A.; Rodicio, I.; Humphry-Baker, R.; Mueller, E.; Liska, P.; Vlachopoulos, N.; Grätzel, M. Conversion of Light to Electricity by *cis*-X_2Bis(2,2′-bipyridyl-4,4′-dicarboxylate)-ruthenium(II) Charge-Transfer Sensitizers (X = $C1^-$, Br^-, I^-, CN^-, and SCN^-) on Nanocrystalline TiO_2 Electrodes. *J. Am. Chem. Soc.* **1993**, *115*, 6382−6390.
(41) Zhao, J.; Shen, X.; Yan, F.; Qiu, L.; Lee, S.; Sun, B. Solvent-free Ionic Liquid/Poly(ionic liquid) Electrolytes for Quasi-Solid-State Dye-Sensitized Solar Cells. *J. Mater. Chem.* **2011**, *21*, 7326−7330.
(42) Wang, X.; Deng, R.; Kulkarni, S.; Wang, X.; Pramana, S. S.; Wong, C. C.; Grätzel, M.; Uchida, S.; Mhaisalkar, S. G. Investigation of the Role of Anions in Hydrotalcite for Quasi-Solid State Dye-Sensitized Solar Cells Application. *J. Mater. Chem. A* **2013**, *1*, 4345−4351.
(43) Fabregat-Santiago, F.; Bisquert, J.; Palomares, E.; Otero, L.; Kuang, D.; Zakeeruddin, S.; Grätzel, M. Correlation between Photovoltaic Performance and Impedance Spectroscopy of Dye-Sensitized Solar Cells Based on Ionic Liquids. *J. Phys. Chem. C* **2007**, *111*, 6550−6560.
(44) Wang, Q.; Moser, J. E.; Grätzel, M. Electrochemical Impedance Spectroscopic Analysis of Dye-Sensitized Solar Cells. *J. Phys. Chem. B* **2005**, *109*, 14945−14953.
(45) Fabregat-Santiago, F.; Bisquert, J.; Garcia-Belmonte, G.; Boschloo, G.; Hagfeldt, A. Influence of Electrolyte in transport and Recombination in Dye-Sensitized Solar Cells Studied by Impedance Spectroscopy. *Sol. Energy Mater. Sol. Cells* **2005**, *87*, 117−131.
(46) Hou, Q.; Zheng, Y.; Chen, J. F.; Zhou, W.; Deng, J.; Tao, X. Visible-Light-Response Iodine-Doped Titanium Dioxide Nanocrystals for Dye-Sensitized Solar Cells. *J. Mater. Chem.* **2011**, *21*, 3877−3883.

DOI: 10.1021/acsami.5b06035
ACS Appl. Mater. Interfaces 2015, 7, 21381−21390